Original Article

Journal of Tissue Engineering
Volume 9: 1–14
© The Author(s) 2018
Reprints and permissions:
sagepub.co.uk/journalsPermissions.nav
DOI: 10.1177/2041731418781696
journals.sagepub.com/home/tej
SAGE

The importance of factorial design in tissue engineering and biomaterials science: Optimisation of cell seeding efficiency on dermal scaffolds as a case study

Alexandra Levin[1], Vaibhav Sharma[1], Lilian Hook[2] and Elena García-Gareta[1]

Abstract

This article presents a case study to show the usefulness and importance of using factorial design in tissue engineering and biomaterials science. We used a full factorial experimental design ($2 \times 2 \times 2 \times 3$) to solve a routine query in every biomaterial research project: the optimisation of cell seeding efficiency for pre-clinical in vitro cell studies, the importance of which is often overlooked. In addition, tissue-engineered scaffolds can be cellularised with relevant cell type(s) to form implantable tissue constructs, where the cell seeding method must be reliable and robust. Our results show the complex relationship between cells and scaffolds and suggest that the optimum seeding conditions for each material may be different due to different material properties, and therefore, should be investigated for individual scaffolds. Our factorial experimental design can be easily translated to other cell types and three-dimensional biomaterials, where multiple interacting variables can be thoroughly investigated for better understanding of cell–biomaterial interactions.

Keywords

Factorial design, biomaterials, tissue engineering, cell seeding efficiency, dermal scaffolds, dermal fibroblasts

Date received: 20 February 2018; accepted: 15 May 2018

Introduction

The demand for tissue-engineered dermal scaffolds for treating full thickness skin wounds continues to rise as healthcare standards increase the life expectancy of patients and current products present limitations, such as unreliable integration and high costs.[1–3] Skin is made up of two main layers: the epidermis, which is closest to the surface, and the dermis. These layers contain sub-layers composed of highly organised and regulated cell types. Following a superficial wound, cells migrate towards the site of damage and up towards the skin surface where they flatten, harden and form the outermost protective layer of the skin. This essential migration is possible because cells are surrounded and held in place by the extracellular matrix (ECM). Wound healing is a meticulous and organised process which must balance cell growth and cell death.[4] However, in individuals with reduced capacity to heal or in the case of full thickness skin wounds where both the epidermis and the dermis are lost, wound healing is disrupted. The body's intrinsic wound healing mechanism is therefore not always sufficient in mediating a full recovery. Tissue-engineered dermal scaffolds support the body through the wound healing process by providing an alternative ECM structural support to which cells such as fibroblasts can attach, infiltrate, proliferate and finally aid

[1]Regenerative Biomaterials Group, RAFT Institute, Northwood, UK
[2]Smart Matrix Ltd, Northwood, UK

Corresponding author:
Elena García-Gareta, Regenerative Biomaterials Group, RAFT Institute, Leopold Muller Building, Mount Vernon Hospital, Northwood HA6 2RN, UK.
Email: garciae@raft.ac.uk

in the breakdown of the biodegradable scaffold so that no trace remains.[1–3,5]

Through studying the components required to heal a wound, different compounds and combinations of naturally occurring materials have been selected to make dermal scaffolds. As an example, the commercially available and clinically well-established Integra® is a three-dimensional (3D) cross-linked porous matrix made of bovine tendon collagen type I with 10%–15% chondroitin-6-sulphate derived from shark cartilage and a silicone backing layer.[6–8] Integra owes its wound healing capabilities to the collagen type I molecule, the main component of the skins' natural ECM, as well as its ability to recognise and interact with antigens on the surface of skin cells.[9–11] Another example is Smart Matrix®, which is currently under development and is a 3D cross-linked porous matrix of fibrin and alginate.[12–14] Fibrin is crucial to the wound healing process as it plays an active role in physiological repair and in the re-infiltration of both cells and blood vessels.[15,16]

Dermal scaffolds, as with other biomaterials intended for tissue repair or regeneration, undergo rigorous in vitro and in vivo testing to fine tune their optimal properties for efficient wound healing.[17–20] In vitro pre-clinical studies serve as an essential intermediate between the conception of a scientific idea and in vivo testing and final translation into the clinic. Many in vitro studies involve seeding cells onto such biomaterials to investigate cell–scaffold interactions.[12,19,21,22] In addition, scaffolds can be cellularised with relevant cell type(s) to form implantable tissue constructs.[5,23,24] Therefore, the cell seeding method used in these various instances must be reliable and robust.

Static cell seeding is the most commonly used method. However, many factors such as cell density, seeding time and cell culture substrate can affect the cell seeding efficiency, which is often overlooked.[25,26] This slows experiments and can be costly in terms of resources and time. Optimising factors required for maximal cell seeding efficiency could limit the number of cells lost during scaffold seeding, make in vitro cell studies more cost-effective and help in the research and development of new biomaterials for tissue reconstruction, including skin wound healing. Traditionally, optimisation of cell seeding efficiency has been done by varying one-factor-at-a-time (OFAT) where it is assumed that the different factors are independent of each other.[25–28] Therefore, interaction of factors is not studied. Moreover, OFAT experiments are time-consuming. Design of experiments (DOE) offers a tool to develop an efficient multi-factor experimental strategy that ensures that all factors and their interactions are systematically investigated. DOE is routinely applied to the optimisation and development of processes in a broad range of industries and scientific fields such as biopharmaceutical manufacturing, stem cell biology and drug discovery.[29–31] However, its application in the fields of biomaterial development and tissue engineering is still limited, although some examples can be found in the literature.[32–34]

The aim of this study was to optimise the cell seeding efficiency on dermal scaffolds for in vitro pre-clinical studies using full factorial design, a type of DOE. Specifically, four factors or variables were investigated per scaffold: (1) cell passage number, (2) cell seeding density, (3) scaffold disc to well plate surface area ratio and (4) attachment incubation time. Primary normal human dermal fibroblasts were used in this study as they are the main cell type found in the dermis.[35] Two different dermal scaffolds, Integra and Smart Matrix, were used. We hypothesised that the interaction(s) of variables that affect cell seeding efficiency is different for each dermal scaffold. The overall objective of this case study was to highlight the importance and usefulness of factorial design in the tissue engineering and biomaterials fields.

Materials and methods

Experimental design

Cells chosen for this investigation were primary normal human dermal fibroblasts as implanted dermal scaffolds are infiltrated with this cell subtype. Two different dermal substitutes were used: the commercially available and clinically well-established Integra and Smart Matrix which is manufactured in our laboratory and is currently undergoing clinical testing.[12–14] Variables and levels investigated were as follows: (1) cell passage number (5 or 10); (2) cell seeding density (1.25×10^5, 2.5×10^5, or 5×10^5 cells in 200 µL), (3) scaffold disc to well plate surface area ratio (1:1 or 1:6); (4) attachment incubation time (3 or 24 h). The rationale for the chosen cell seeding densities was based on our previous and extensive experience with these materials:[12–14] the maximum number of cells that can be seeded per 6-mm-diameter disc of material is 5×10^5. Seeding a higher number of cells does not result in more cells attaching to the materials. Similarly, we know from experience that the other chosen variables affect the cell seeding efficiency on these scaffolds.[12–14] A full factorial experimental design was used ($2 \times 2 \times 2 \times 3$). A matrix of variables and levels was created (Figure 1) and for each individual set of experimental conditions, three replicates were performed ($n = 3$). This allowed us to observe the effect of the interaction of variables on cell seeding efficiency, which was quantitatively assessed using alamarBlue®, a metabolic redox assay. Resazurin, the blue, non-fluorescent component of alamarBlue is reduced by electrons carried along the electron transport chain within metabolising cells. Subsequent reduction of blue Resazurin to fluorescent pink Resorufin does not interfere with cell signalling, but the change in absorbance can be assessed.[36]

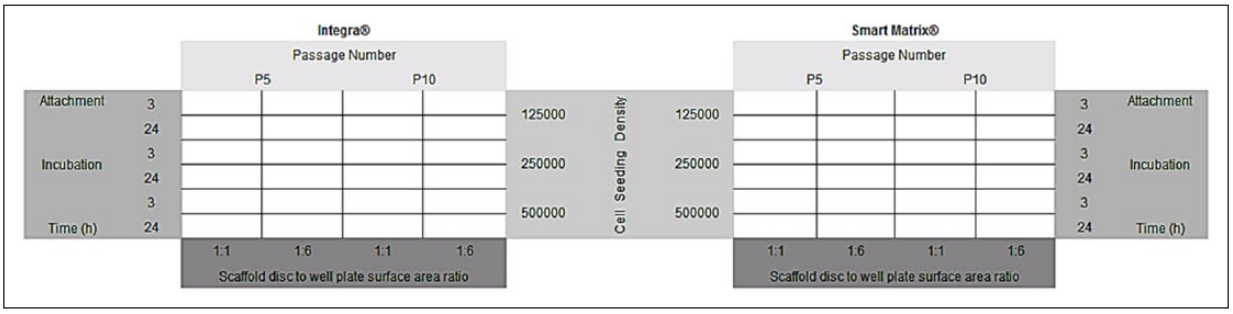

Figure 1. Matrix of variables investigated in this study along with levels for each variable. For each individual set of experimental conditions n = 3.

A standard curve was created as a point of reference for each passage number and attachment incubation time. This allowed calculation of the number of cells on the dermal scaffolds after the attachment incubation time as a comparative percentage of total cells seeded. Cell seeding efficiency was calculated and is presented as percentage of cells remaining on the scaffolds. Furthermore, cell seeding was qualitatively assessed by histological processing and microscopy to observe both cells attached to the tissue culture plates after seeding and cells adhered to the scaffolds.

Dermal scaffolds

Two dermal scaffolds were used in this study: (1) Integra, a 2.1-mm-thick bilayer of bovine tendon collagen type 1/chondroitin-6-sulphate cross-linked with glutaraldehyde and a silicone backing; (2) bovine Smart Matrix, a 2-mm-thick freeze-dried layer of bovine fibrin/alginate cross-linked with glutaraldehyde.

The dermal scaffolds were imaged by scanning electron microscopy (SEM). Specimens were mounted on stubs, gold sputtered coated (Agar Auto Sputter Coater, Agar Scientific, UK) and observed (FEI Inspect F, Oxford Instruments, UK). Wetting of the two different dermal scaffolds, which affects retention of cell suspension, was assessed with a simple experiment. Dermal scaffolds were cut into 6-mm-diameter discs (Figure 2(a)) using a cork borer and individually placed at the centre of the wells of a 6-well plate. Increasing volumes (25 µL) of phosphate buffered saline (PBS) were added to the scaffolds and the capacity of the scaffolds to retain the PBS was visually observed and photographed using an iPhone 6+ digital camera.

Cell culture

Primary normal human dermal fibroblasts (pnHDFs) from a single donor were established from routine surgical excision of normal skin, obtained with informed consent and local ethics committee approval.[12–14] Cells were cultured in Dulbecco's modified Eagles' medium (DMEM, 31885-023, Gibco, UK; Lot 1683048 used throughout this study) supplemented with 10% foetal bovine serum (FBS, 10270-106, Gibco; Lot 41Q3446K used throughout this study), 10 U/mL of penicillin/streptomycin (15140-122, Gibco) and 200 µL of L-glutamine (25030-024, Gibco) at 37°C with 5% CO_2. Cell media were changed every 3 days and cells were passaged at ~80% confluency. Cells were routinely observed by phase-contrast light microscopy (Nikon Eclipse TS100) and photographed using a Leica DC200 digital camera and IC50 software. For this study, pnHDFs were used at passages 5 or 10 (P5 or P10).

Ki67 expression

To confirm that the cells were proliferative at the time of the experiment, immunostaining of the cell proliferation marker Ki67 was carried out. 1×10^4 pnHDFs were seeded on 13-mm-diameter borosilicate glass coverslips (631-0150; VWR International, UK) and cultured for 24 h at 37°C with 5% CO_2. Cells were fixed in 4% paraformaldehyde. Fixed samples were washed twice with PBS, permeabilised with two drops of 0.5% Triton X-100 in PBS for 5 min at room temperature, washed three times with PBS and incubated in block buffer (0.5% bovine serum albumin (BSA) in PBS, pH 7.4) for 30 min at room temperature. After draining the block buffer into tissue paper, samples were incubated with mouse anti-rat Ki67 antigen (M7248, Dako; 1:100 in block buffer) for 1 h at room temperature inside a dark humidified chamber. The primary antibody was drained off and samples were washed five times with wash buffer and once with PBS. Samples were incubated with a secondary antibody (goat anti-mouse Alexa Fluor® 546, A11003, Invitrogen™, USA; 1:100 in block buffer) and phalloidin (Alexa Fluor 488 phalloidin, A12379, Invitrogen, USA; 1:100 in block buffer) for 1 h at room temperature inside a dark humidified chamber, washed three times in wash buffer (0.1% Triton X-100 and 0.1% BSA/PBS, pH 7.4), then once in PBS and once in distilled water. Samples were transferred to slides with one drop of Vecta Mount™ (H-5000; Vector, USA) and viewed under a confocal laser microscope (LEICA DMIRE2; Leica, Germany).

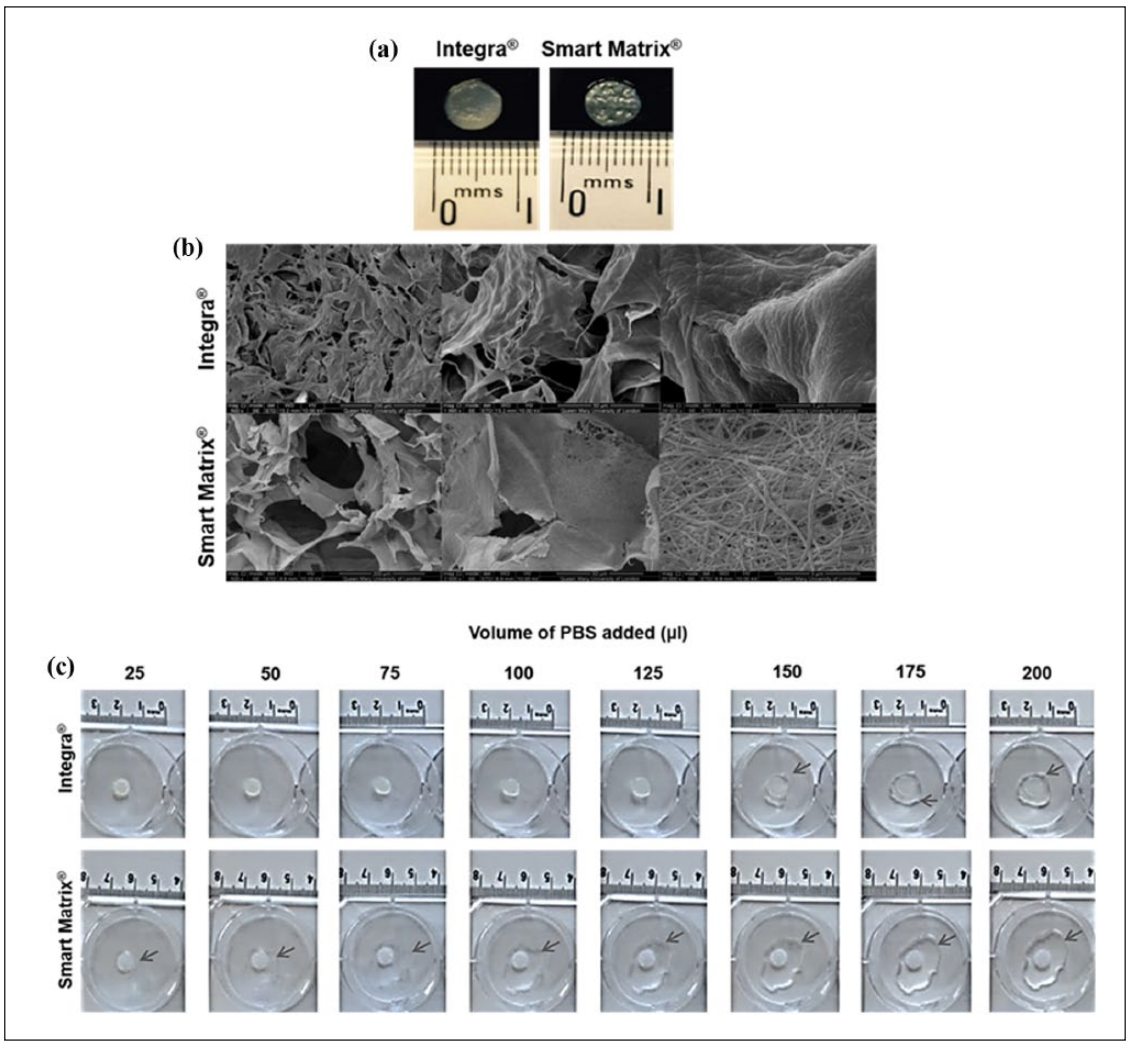

Figure 2. Dermal scaffolds used in this study. (a) Macroscopic view of 6 mm discs used. (b) SEM images. (c) Wetting of the dermal scaffolds (arrows point at liquid not retained by the scaffolds).

Cell seeding on dermal scaffolds

Dermal scaffolds were cut into 6-mm-diameter discs using a cork borer and individually placed in either a flat-bottom 96-well plate, where they tightly fit (1:1 area ratio), or in a flat-bottom 24-well plate (1:6 area ratio). Before cell seeding, a viable cell count was performed using trypan blue (T8154; Sigma-Aldrich, UK) to establish the percentage of viability of the cells. pnHDFs were seeded at different densities (1.25×10^5, 2.5×10^5 or 5×10^5 in 200 µL) onto dermal scaffolds placed in 96- or 24-well plates. Plates were incubated for either 3 or 24 h at 37°C with 5% CO_2. Following incubation, seeded scaffolds were transferred to new 24-well plates and an alamarBlue metabolic activity assay was carried out. Cells left on the well plates where the cell seeding took place were observed by phase-contrast light microscopy (Nikon Eclipse TS100) and photographed using a Leica DC200 digital camera and IC50 software.

Standard curves

For both P5 and P10, standard curves were produced. pnHDFs were seeded at densities ranging from 1×10^3 to 1×10^6 in well plates and incubated for either 3 or 24 h at 37°C with 5% CO_2. Following incubation, an alamarBlue activity assay was carried out.

alamarBlue activity assay

1 mL of 10% alamarBlue (DAL1025, Invitrogen, UK; Lot 500143 used throughout this study) stock diluted into phenol-free supplemented DMEM (11880, Gibco; Lot 1640664 used throughout this study) was added per well and incubated at 37°C with 5% CO_2 for 2 h. For each sample, 1 mL was transferred to a cuvette (FB55147; Fisher Scientific, UK) and following the manufacturer's instructions, absorbance at 570 nm was measured against air using a M550 double beam ultraviolet (UV)/visible

Table 1. Summary of structural parameters for the scaffolds Integra® and Smart Matrix®.

Parameter	Integra	Smart Matrix
Average porosity (% Vol)	90.02	83.22
Pore interconnectivity (%)	100	100
Average pore size (μm)	158.61	132.26
Average roughness Sa (nm)	75.565	114.776
Average G′ (kPa)	313.74	8.26

spectrophotometer (Camspec, UK). Absorbance at 600 nm of phenol-free DMEM was measured and subtracted from sample values. After the assay, seeded dermal scaffolds were fixed in 4% paraformaldehyde for paraffin histology.

Histology

Fixed specimens in 4% paraformaldehyde were embedded in paraffin. Sections (4 μm) were taken for haematoxylin and eosin (H&E) staining and viewed under light microscopy (Zeiss Axiophot, UK) with a DC200 Leica digital camera and IC50 software.

Statistical analysis

Statistical analysis was done with Microsoft Excel 2016 software using a two-way analysis of variance (ANOVA) with replication test (alpha = 0.05).

Results

Dermal scaffolds

Dermal scaffolds were visually characterised by SEM (Figure 2(b)). Both have a homogeneous structure of open, interconnected pores, which has been shown to be essential for nutrient and oxygen delivery as well as for waste removal from the scaffold, so cell migration and growth are not inhibited.[37,38] Scaffolds should also provide a homogeneous environment for cell growth and migration to avoid cell gradients that would result in non-homogeneous tissue growth.[37,38] Both dermal scaffolds displayed micro-pores; however, nano-pores and densely packed nano-fibres were only observed for Smart Matrix. Nano-structural features of scaffolds for tissue regeneration are important as they more closely resemble the native ECM that cells encounter in vivo.[39–42] The structural parameters of both scaffolds (Table 1), calculated in a previous study by our group,[13] show their similarities, with Integra having a slightly higher porosity than Smart Matrix, while the latter presents a higher surface roughness compared to Integra. The main difference between the scaffolds is in the rheological properties: while both can be described as viscoelastic solids (like skin tissue), Integra is mechanically stronger than Smart Matrix due to the presence of the silicone backing layer.[13]

Wetting of the scaffolds was assessed using a simple experiment where increasing volumes (25 μL) of PBS were added to the scaffolds. The capacity of the biomaterials to retain the liquid was observed and photographed (Figure 2(c)). It was found that Integra was capable of retaining larger volumes of liquid of up to 125 μL, while Smart Matrix barely retained 25 μL. This stark difference between the scaffolds may be due to the presence of a hydrophobic silicone backing layer in Integra. This suggests that Integra could retain cell suspensions in a similar way, thus influencing cell seeding efficiency.

Cells

pnHDFs under phase-contrast light microscopy (Figure 3(a)) displayed the typical spindle-shaped morphology, with branched cytoplasm, characteristic of fibroblasts. Cells had an elliptical nucleus containing two or more nucleoli and visible rough endoplasmic reticulum. pnHDFs appeared scattered and disjointed at low confluency but often aligned in parallel clusters when confluent. Cells connected through visible cytoplasmic processes. We believe that routine monitoring of the morphology of primary cells is necessary as a quality control measure before they can be used for experimentation. Primary cells are directly isolated from tissues and as such their behaviour represents their native tissue, but they can only be cultured for a certain number of passages before they become senescent, which marks the end of their proliferative capacity.[43] Senescent dermal fibroblasts are easily detected under light microscopy as they lose their original morphology and become larger with distinct intracellular features such as increased number of vacuoles.[43] The cells used for this study retained the typical morphology of human dermal fibroblasts throughout (Figure 3(a)). Moreover, percentage viability of cells at P5 and P10 was consistently higher than 97%, although slightly lower for P10 cells as expected (Figure 3(b)). Immunostaining using a specific antibody against Ki67 followed by confocal imaging reaffirmed that the cells used in this study were actively proliferative (Figure 3(a)). The cells used for this study were kept in culture up to P14, where the senescent features described above were observed and cell proliferation was clearly stalled.

Cell seeding efficiency: main effects and interactions

Cell seeding efficiency was calculated as the percentage of cells present on the scaffolds after the seeding and attachment incubation procedure. It is worth noting that in this study, an efficiency of 0% means that fewer than 1×10^3 cells were attached to the material. Results displayed in

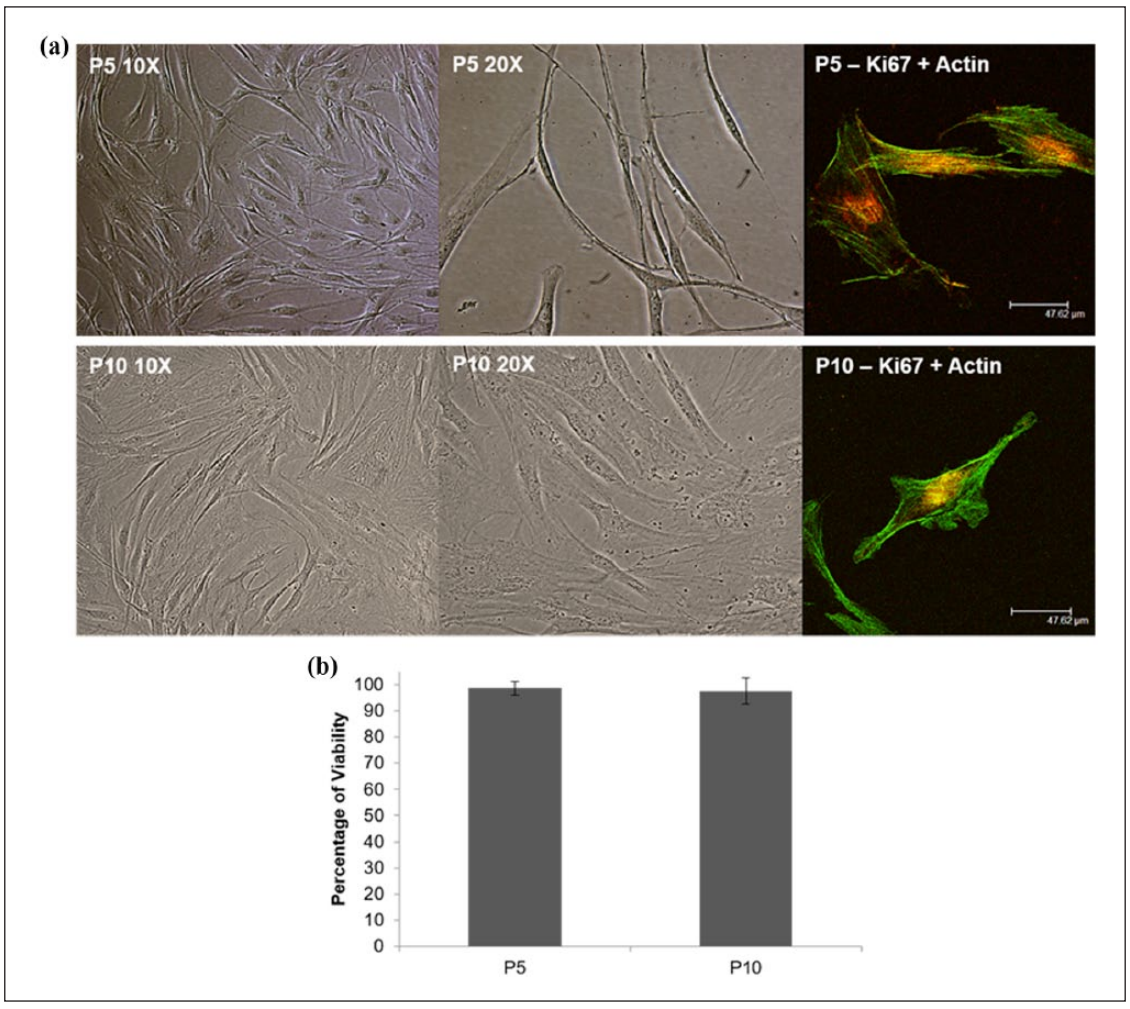

Figure 3. (a) Representative phase-contrast light microscopy and confocal microscopy images of primary normal human dermal fibroblasts used in this study, showing that cells maintained their spindle-shaped morphology throughout the study. Confocal images of immunostained cells for Ki67 (red) and actin (green) shows expression of the proliferation marker Ki67 in the cells' nucleus suggesting they were proliferative at the time of the experiments. (b) Percentage of viability graph shows average ± standard deviation.

Figure 4(a) show that the percentage of cells attached to the scaffolds was affected by the different variables investigated.

In terms of cell passage number, results show that in general, higher efficiencies were obtained at P5 compared with P10 for both 3 and 24 h incubation times (Figure 4(a)). Numerous studies have shown that cells suffer morphological, biochemical and functional alterations as the cell passage increases, which affects their proliferative and migratory capacities.[44,45] Regarding cell seeding density, a trend was seen for Smart Matrix at both P5 and P10 for 3 h incubation time independently of the scaffold disc to well plate surface area ratio: as the cell density increases, the cell seeding efficiency decreases. The trend was not observed for 24 h incubation time which suggests a strong influence of incubation time on cell seeding efficiency. For Integra, the trend discussed for Smart Matrix was only observed for the 1:6 scaffold disc to well plate surface area ratio for 3 h incubation time at both P5 and P10, while it was reversed for 1:1 scaffold disc to well plate surface area ratio. It is worth noting that for both scaffolds, the highest efficiencies were obtained at the lowest cell seeding density (1.25×10^5) for both P5 and P10, suggesting that reducing cell crowding in the cell seeding suspension may increase the cell seeding efficiency or the existence of a saturation point, that is, only a certain number of cells can attach to the scaffolds.

Higher efficiencies were observed for both dermal scaffolds for the 1:1 scaffold disc to well plate surface area ratio for both 3 and 24 h incubation time at both passage numbers (Figure 4(a)). Within the 24-well plate (1:6) there was a larger non-dermal scaffold surface area for cell attachment, whereas within the 96-well plate (1:1) cells were effectively forced onto the dermal scaffolds by physical limitation within the well. Interestingly, differences were less pronounced for Integra than for Smart Matrix, which

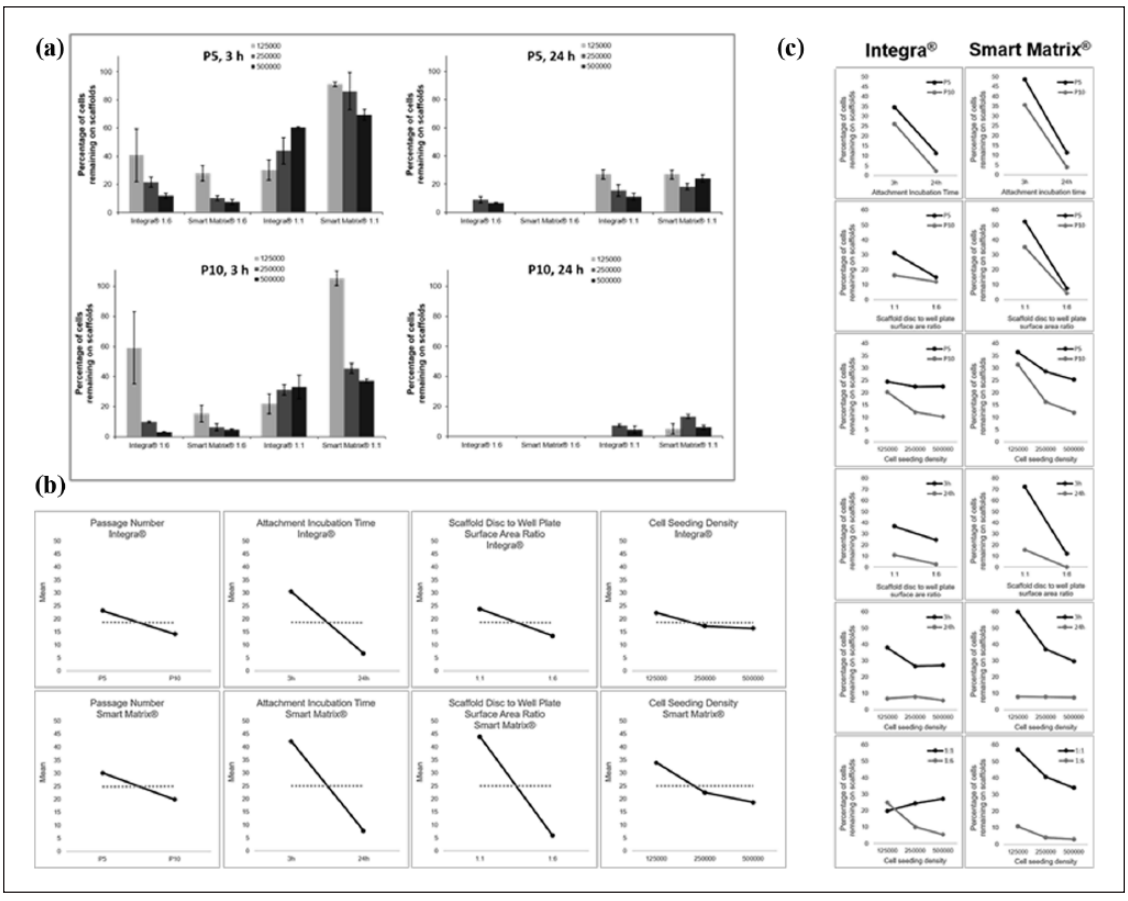

Figure 4. (a) Cell seeding efficiency on both dermal scaffolds under the four different variables investigated in this study. Results show average ± standard error mean. (b) Main effect plots. (c) Two-factor interaction plots.

may be due to the different wetting properties of both materials: Integra is able to retain larger volumes of liquid than Smart Matrix (Figure 3(c)). Therefore, cells in the cell seeding suspension are more likely to be in contact with the material scaffold if seeded on Integra than if seeded on Smart Matrix. These results suggest that the material's properties are important when optimising the cell seeding efficiency. Moreover, it should be mentioned that the cell seeding volume used in this study was quite large (200 µL): using a smaller volume would decrease the effect of the scaffold disc to well plate surface area ratio factor. Finally, a strong influence of the attachment incubation time variable was observed for both dermal scaffolds as higher efficiencies were measured after 3 h incubation compared to 24 h incubation. This may be due to media evaporation, resulting in cell lysis with increasing incubation time.[27]

Main effect plots (Figure 4(b)) confirmed the strong negative effect of the attachment incubation time variable on seeding efficiency. Similarly, scaffold disc to well plate surface area ratio had a strong negative effect for Smart Matrix, while its negative effect was not strong for Integra as previously observed from the data displayed in Figure 4(a). Increasing passage number had a negative effect for both scaffolds, although it was not as strong as the aforementioned variables. Finally, increasing cell seeding density also had a negative effect on the seeding efficiency. The effect was larger for Smart Matrix than for Integra and larger when increasing from 1.25×10^5 to 2.5×10^5 than when increasing from 2.5×10^5 to 5×10^5. However, overall, this variable seemed to have the least strong effect on seeding efficiency of all the factors investigated in this study.

Two-factor interaction plots (Figure 4(c)) suggested multiple interactions for both materials. Statistical analysis of these results showed that for Smart Matrix (Table 2), the main effects of attachment incubation time and scaffold disc to well plate surface area ratio were statistically significant and so was their interaction. However, for Integra (Table 3), only the main effect of attachment incubation time was statistically significant while none of the interactions suggested by the two-factor plots were significant.

Microscopy

The next part of this study involved visual confirmation of the results previously described and discussed. Phase-contrast light microscopy of empty wells (after transferring the seeded scaffolds to new wells for the alamarBlue

Table 2. Two-way ANOVA statistical analysis of results for Smart Matrix.

Passage number/attachment incubation time						
Source of variation	SS	df	MS	F	P-value	F crit
Passage number	627.5196297	1	627.5196	0.814573	0.377513	4.351244
Attachment incubation time	7110.063006	1	7110.063	9.229461	**0.006495**	4.351244
Interaction	47.89944573	1	47.89945	0.062178	0.80563	4.351244
Within	15,407.31953	20	770.366	–	–	–
Total	23,192.80162	23	–	–	–	–
Passage number/scaffold disc to well plate surface area ratio						
Source of variation	SS	df	MS	F	P-value	F crit
Passage number	627.5196297	1	627.5196	0.923124	0.348129	4.351244
Scaffold disc/well plate surface area	8676.122015	1	8676.122	12.76316	**0.001906**	4.351244
Interaction	293.5879223	1	293.5879	0.431888	0.518556	4.351244
Within	13,595.57205	20	679.7786	–	–	–
Total	23,192.80162	23	–	–	–	–
Passage number/cell seeding density						
Source of variation	SS	df	MS	F	P-value	F crit
Passage number	627.5196297	1	627.5196	0.526167	0.477548	4.413873
Cell seeding density	1016.717587	2	508.3588	0.426252	0.659373	3.554557
Interaction	81.33679455	2	40.6684	0.0341	0.966537	3.554557
Within	21,467.2276	18	1192.624	–	–	–
Total	23,192.80162	23	–	–	–	–
Scaffold disc to well plate surface area ratio/attachment incubation time						
Source of variation	SS	df	MS	F	P-value	F crit
Scaffold disc/well plate surface area	8676.122015	1	8676.122	39.54241	**3.87E-06**	4.351244
Attachment incubation time	7110.063006	1	7110.063	32.40492	**1.43E-05**	4.351244
Interaction	3018.355262	1	3018.355	13.7565	**0.001388**	4.351244
Within	4388.261333	20	219.4131	–	–	–
Total	23,192.80162	23	–	–	–	–
Attachment incubation time/cell seeding density						
Source of variation	SS	df	MS	F	P-value	F crit
Attachment incubation time	7110.063006	1	7110.063	9.077012	**0.007474**	4.413873
Cell seeding density	1016.717587	2	508.3588	0.648993	0.534373	3.554557
Interaction	966.542881	2	483.2714	0.616965	0.550605	3.554557
Within	14,099.47814	18	783.3043	–	–	–
Total	23,192.80162	23	–	–	–	–
Scaffold disc to well plate surface area ratio/cell seeding density						
Source of variation	SS	df	MS	F	P-value	F crit
Scaffold disc/well plate surface area	8676.122015	1	8676.122	11.77456	**0.002977**	4.413873
Cell seeding density	1016.717587	2	508.3588	0.689905	0.514407	3.554557
Interaction	236.6088464	2	118.3044	0.160554	0.852878	3.554557
Within	13,263.35317	18	736.853	–	–	–
Total	23,192.80162	23	–	–	–	–

ANOVA: analysis of variance.
Cells in bold font indicate statistical significances.

Table 3. Two-way ANOVA statistical analysis of results for Integra.

Passage number/attachment incubation time						
Source of variation	SS	df	MS	F	P-value	F crit
Passage number	484.5211	1	484.5211	2.472838	0.131515	4.351244
Attachment incubation time	3398.534	1	3398.534	17.34501	**0.000479**	4.351244
Interaction	1.819892	1	1.819892	0.009288	0.924182	4.351244
Within	3918.745	20	195.9372	–	–	–
Total	7803.62	23	–	–	–	–
Passage number/scaffold disc to well plate surface area ratio						
Source of variation	SS	df	MS	F	P-value	F crit
Passage number	484.5211	1	484.5211	1.499572	0.234966	4.351244
Scaffold disc/well plate surface area	643.4712	1	643.4712	1.991515	0.17355	4.351244
Interaction	213.5006	1	213.5006	0.660775	0.425858	4.351244
Within	6462.127	20	323.1063	–	–	–
Total	7803.62	23	–	–	–	–
Passage number/cell seeding density						
Source of variation	SS	df	MS	F	P-value	F crit
Passage number	484.5211	1	484.5211	1.232061	0.281616	4.413873
Cell seeding density	168.6802	2	84.34012	0.214464	0.809007	3.554557
Interaction	71.72611	2	35.86305	0.091194	0.91326	3.554557
Within	7078.692	18	393.2607	–	–	–
Total	7803.62	23	–	–	–	–
Scaffold disc to well plate surface area ratio/attachment incubation time						
Source of variation	SS	df	MS	F	P-value	F crit
Scaffold disc/well plate surface area	3398.534	1	3398.534	18.18749	**0.000379**	4.351244
Attachment incubation time	643.4712	1	643.4712	3.443581	0.078296	4.351244
Interaction	24.3927	1	24.3927	0.130539	0.721662	4.351244
Within	3737.222	20	186.8611	–	–	–
Total	7803.62	23	–	–	–	–
Attachment incubation time/cell seeding density						
Source of variation	SS	df	MS	F	P-value	F crit
Attachment incubation time	3398.534	1	3398.534	15.0631	**0.001095**	4.413873
Cell seeding density	168.6802	2	84.34012	0.373815	0.693322	3.554557
Interaction	175.2495	2	87.62473	0.388373	0.683706	3.554557
Within	4061.156	18	225.6198	–	–	–
Total	7803.62	23	–	–	–	–
Scaffold disc to well plate surface area ratio/cell seeding density						
Source of variation	SS	df	MS	F	P-value	F crit
Scaffold disc/well plate surface area	643.4712	1	643.4712	1.862794	0.189122	4.413873
Cell seeding density	168.6802	2	84.34012	0.244157	0.785917	3.554557
Interaction	773.6681	2	386.834	1.119851	0.348029	3.554557
Within	6217.8	18	345.4334	–	–	–
Total	7803.62	23	–	–	–	–

ANOVA: analysis of variance.
Cells in bold font indicate statistical significances.

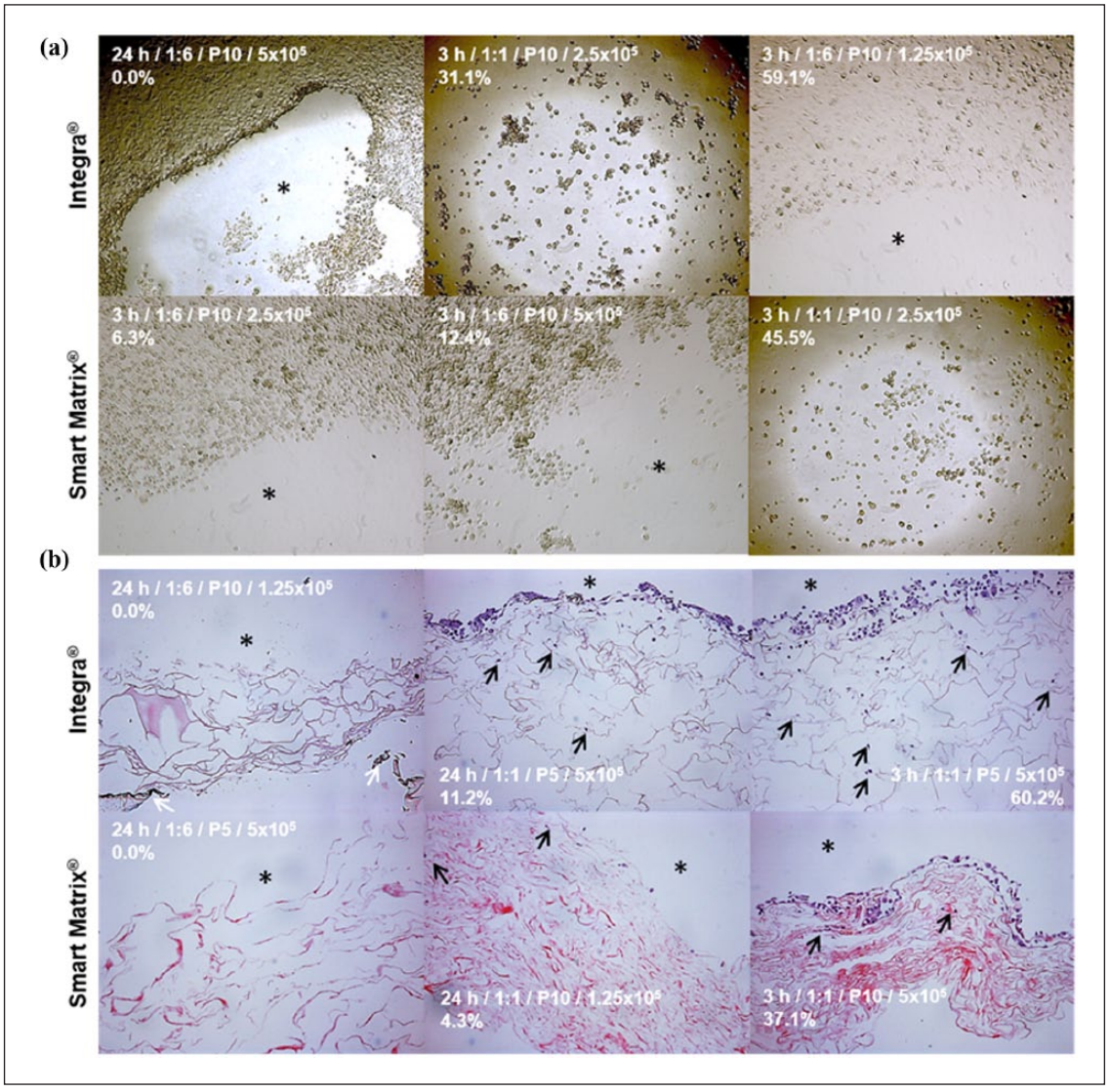

Figure 5. (a) Phase-contrast light microscopy photos (4× magnification) of cells left on empty wells after the cell seeding procedure (* highlights the area where the scaffold was placed). (b) Light microscopy photos (10× magnification) of H&E stained seeded scaffolds with the scaffold stained pink and the cells stained purple (* indicates top of scaffold where the cells were seeded onto; white arrows point at remaining silicone layer of Integra which mostly separated from the matrix during histological processing; black arrows point to cells that migrated into the scaffolds).

assay) revealed a ring of cells left behind following scaffold removal from 24-well plates (Figure 5(a)). Fewer cells were left behind in 96-well plates, which appeared more uniformly distributed throughout the wells (Figure 5(a)). These results agree with those from the alamarBlue assay and confirm that using a 96-well plate restricts cell seeding adhesion to the scaffold and thus less cells are wasted by physically limiting them to attach to the scaffold. H&E staining of seeded scaffolds revealed a layer of cells at the top of the scaffold where they were seeded (Figure 5(b)). Images also revealed that at 3 h of incubation, cells had already started to penetrate through the scaffold matrices, an essential feature for tissue reconstruction as cells need to attach and penetrate through the scaffold to produce new tissue.[1] Qualitatively fewer cells were observed as the seeding efficiency decreased.

Visual representation of results

Finally, in order to more clearly observe the effects and interactions of the different variables and find the optimum combinations that should be used for each scaffold, we propose two different visual representations of the data presented in Figure 4: in the first representation, data were plotted in 3D graphs (Figure 6(a)), while the second, the matrix depicted in Figure 1, was filled with results from this study and a colour key was assigned to values (Figure 6(b)). These two visual representations of the data offer a

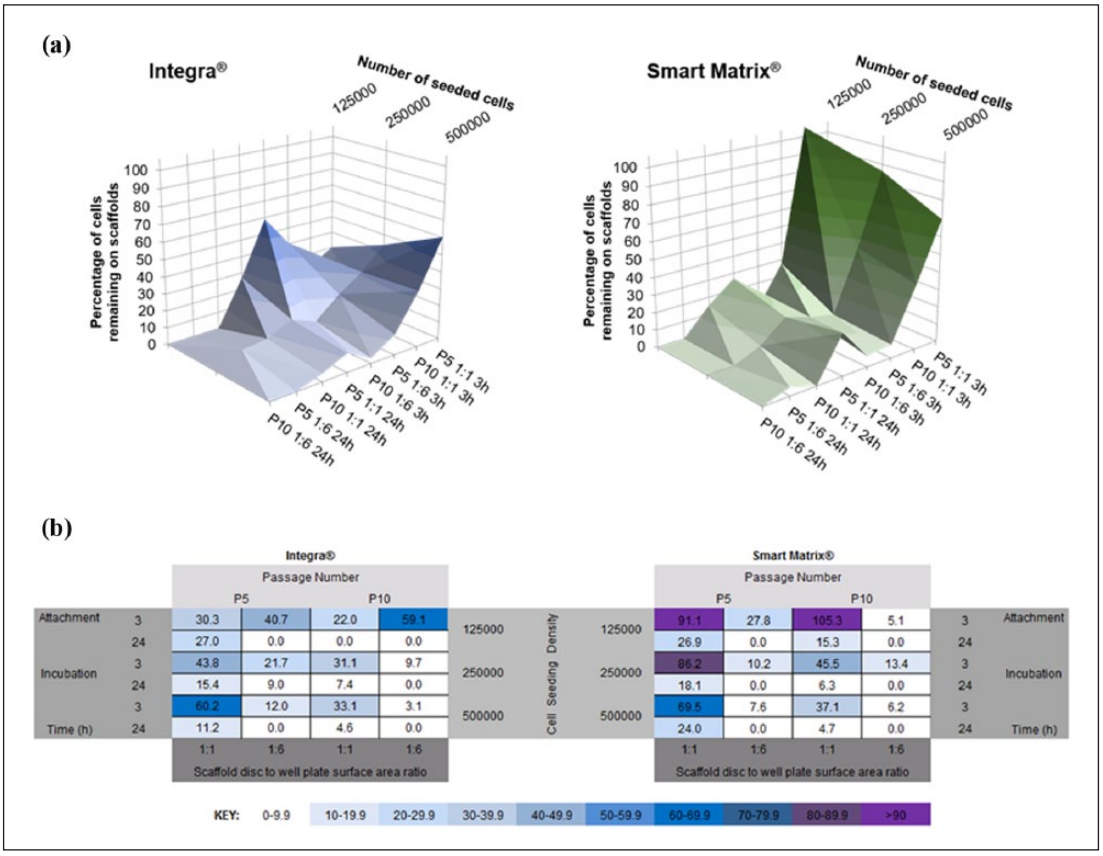

Figure 6. (a) 3D visual representation of cell seeding efficiency on both dermal scaffolds under the four different variables investigated in this study. Results show average values. (b) Matrix of variables showing how combination of the different variables investigated in this study affects cell seeding efficiency, calculated as percentage of cells remaining on the scaffolds. Values show averages for each individual set of conditions.

straightforward and clear understanding of the optimum cell seeding conditions for both scaffolds used in this study. For the collagen-based Integra, highest cell seeding efficiencies were found when (1) 5×10^5 cells at P5 were seeded on scaffolds placed in 96-well plates (1:1) and incubated for 3 h (60.2%), or (2) 1.25×10^5 cells at P10 were seeded on scaffolds placed in 24-well plates (1:6) and incubated for 3 h (59.1%). For the fibrin-based Smart Matrix, highest efficiencies were found when (1) 1.25×10^5 cells at P10 were seeded on scaffolds placed in 96-well plates (1:1) and incubated for 3 h (105.3%) or (2) 1.25×10^5 cells at P5 were seeded on scaffolds placed in 96-well plates (1:1) and incubated for 3 h (91.1%).

Discussion

In view of the results presented in this article, it would be important to define the optimum cell seeding conditions for each particular material, so the same number of cells is attached and meaningful comparisons between materials are drawn. Similarly, in the case of cellularised materials, defining the optimum cell seeding conditions would be important to ensure the required number of cells is attached to the scaffold. Differences observed between the dermal scaffolds used in our study could be due to their different compositions and nano-structures. Fibrin has been demonstrated as a more efficient natural polymer for cell attachment when compared to collagen[16] and the nano-features of Smart Matrix more closely resemble the natural ECM that cells encounter in vivo.[39–42]

Curiously, despite being an intuitive finding, there are very few reports on the literature that based on accompanying supporting data, recommend and/or imply that cell seeding efficiency should be optimised for each particular material.[46–50] None of the found reports used dermal scaffolds. Furthermore, some of the studies cited[46–50] did not report differences between scaffolds in terms of cell seeding efficiency but in terms of other parameters studied. As an example, using titanium scaffolds for bone tissue engineering, Chen and colleagues[46] did not see differences in the cell seeding efficiency but observed changes in cellular spatial distribution throughout the two different chosen scaffolds (regular vs irregular morphology).

The importance of cell seeding efficiency for both preclinical in vitro cell studies or to form tissue-engineered constructs is often overlooked, as shown by the limited

number of studies found in the literature that explore the optimisation of cell seeding efficiency. The vast majority of these optimisation studies usually investigate one or two variables, commonly cell seeding density, static versus dynamic conditions, various dynamic conditions, incubation time and cell culture plate surface chemistry.[25–28,51,52] In our study, we used a full factorial design where we looked at four different variables that were simultaneously varied to observe not only their effect on cell seeding efficiency but also their interactions, if any, with each other. If it was not for the factorial DOE approach, we would not have been able to study the interaction of the four variables. Thus, the value of such approach, which could be used to solve any problem where several interacting variables are at play. This happens often in the fields of tissue engineering and biomaterials science. In order to reduce time and expense, fractional factorial designs can be used instead of full designs. However, where not all possible combinations of variables are run, researchers should be aware that important interactions may be missed.[46]

In conclusion, in this article, we present a case study to show the usefulness and importance of using factorial design in tissue engineering and biomaterials research. We used a full factorial experimental design ($2 \times 2 \times 2 \times 3$) to solve a simple, routine query in every biomaterial research project. This study design could save time and resources that could help in the research and development of new scaffolds for tissue repair or regeneration. Our results show the complex relationship between cells and scaffolds and suggest that the optimum seeding conditions for each material may be different due to different material properties, and therefore, should be investigated for individual materials. We believe that our factorial experimental design can be easily translated to other cell types and 3D biomaterials, where multiple interacting variables can be thoroughly investigated for better understanding cell–biomaterial interactions.

Acknowledgements

The authors would like to thank Mr Russell Bailey at the Nanovision Centre, Queen Mary University of London, for technical support with SEM, Mr Marcus Kang for technical assistance with the wetting experiment and Dr Nupur Kohli for useful discussions.

Declaration of conflicting interests

Dr Lilian Hook is the Chief Scientific Officer of Smart Matrix Limited (SML) while two of the authors, Dr Vaibhav Sharma and Dr Elena García-Gareta, provide services to SML, established to take the dermal replacement scaffold Smart Matrix® through the development stage and onto patients. Dr Sharma and Dr García-Gareta do not get directly paid for these services. The RAFT Institute, which invented and developed Smart Matrix, has a service agreement with SML. Therefore, the time that these two authors spend on services for SML are reimbursed to the RAFT Institute. The authors have no other conflict of interests to declare.

Funding

This work was supported by the Restoration of Appearance and Function Trust (UK, registered charity number 299811).

References

1. Van der Veen VC, Van der Wal MBA, Van Leeuwen MCE, et al. Biological background of dermal substitutes. *Burns* 2010; 36: 305–321.
2. Dieckmann C, Renner R, Milkova L, et al. Regenerative medicine in dermatology: biomaterials, tissue engineering, stem cells, gene transfer and beyond. *Exp Dermatol* 2010; 19: 697–706.
3. Auger FA, Berthod F, Moulin V, et al. Tissue-engineered skin substitutes: from in vitro constructs to in vivo applications. *Biotechnol Appl Biochem* 2004; 39: 263–275.
4. Ravindran N and García-Gareta E. Kerr's coining of apoptosis and its relevance in skin wound healing and fibrosis. *Exp Dermatol* 2015; 24: 99–100.
5. Davison-Kotler E, Sharma V, Kang NV, et al. A new and universal classification system of skin substitutes inspired by factorial design. *Tissue Eng Part B Rev*. Epub ahead of print 12 February 2018. DOI: 10.1089/ten.TEB.2017.0477.
6. Heitland A, Piatkowski A, Noah EM, et al. Update on the use of collagen/glycosaminoglycate skin substitute – six years of experiences with artificial skin in 15 German burn centers. *Burns* 2004; 30(5): 471–475.
7. Groos N, Guillot M, Zilliox R, et al. Use of an artificial dermis (Integra) for the reconstruction of extensive burn scars in children. About 22 grafts. *Eur J Paediatr Surg* 2005; 15(3): 187–192.
8. Dantzer E and Braye FM. Reconstructive surgery using an artificial dermis (Integra): results with 39 grafts. *Br J Plast Surg* 2001; 54(8): 659–664.
9. Chevallay B and Herbage D. Collagen-based biomaterials as 3D scaffold for cell cultures: applications for tissue engineering and gene therapy. *Med Biol Eng Comput* 2000; 38(2): 211–218.
10. García-Gareta E. Collagen gels and the 'Borstein legacy': from a substrate for tissue culture to cell culture systems and biomaterials for tissue regeneration. *Exp Dermatol* 2014; 23: 473–474.
11. Tzeranis DS, Soller EC, Buydash MC, et al. In situ quantification of surface chemistry in porous collagen biomaterials. *Ann Biomed Eng* 2016; 44(3): 803–815.
12. García-Gareta E, Ravindran N, Sharma V, et al. A novel multiparameter in vitro model of three-dimensional cell ingress into scaffolds for dermal reconstruction to predict in vivo outcome. *Biores Open Access* 2013; 2(6): 412–420.
13. Sharma V, Patel N, Kohli N, et al. Viscoelastic, physical, and bio-degradable properties of dermal scaffolds and related cell behaviour. *Biomed Mater* 2016; 11: 055001.
14. Sharma V, Kohli N, Moulding D, et al. Design of a novel two-component hybrid dermal scaffold for the treatment of pressure sores. *Macromol Biosci*. Epub ahead of print 17 November 2017. DOI: 10.1002/mabi.201700185.

15. Whelan D, Caplice N and Clover A. Fibrin as a delivery system in wound healing tissue engineering applications. *J Control Release* 2014; 196: 1–8.
16. Ahmed TAE, Dare EV and Hincke M. Fibrin: a versatile scaffold for tissue engineering applications. *Tissue Eng Part B Rev* 2008; 14(2): 199–215.
17. Zhong SP, Zhang YZ and Lim CT. Tissue scaffolds for skin wound healing and dermal reconstruction. *Nanomed Nanobiotechnol* 2010; 2(5): 510–525.
18. Musson D, McIntosh J, Callon K, et al. The need for thorough in vitro testing of biomaterial scaffolds: two case studies. *Procedia Eng* 2013; 59: 138–143.
19. Ojeh NO, Frame JD and Navsaria HA. In vitro characterization of an artificial dermal scaffold. *Tissue Eng* 2001; 7(4): 457–472.
20. El-Sherbiny I and Yacoub M. Hydrogel scaffolds for tissue engineering: progress and challenges. *Glob Cardiol Sci Pract* 2013; 3: 316–342.
21. Dainiak MB, Allan IU, Savina IN, et al. Gelatin-fibrinogen cryogel dermal matrices for wound repair: preparation, optimisation and in vitro study. *Biomaterials* 2010; 31: 67–76.
22. Helary C, Bataille I, Abed A, et al. Concentrated collagen hydrogels as dermal substitutes. *Biomaterials* 2010; 31(3): 481–490.
23. Yang Y, Yang JT, Chen XH, et al. Construction of tissue-engineered lymphatic vessel using human adipose derived stem cells differentiated lymphatic endothelial like cells and decellularized arterial scaffold: a preliminary study. *Biotechnol Appl Biochem*. Epub ahead of print 5 October 2017. DOI: 10.1002/bab.1618.
24. Agrawal P, Pramanik K, Biswas A, et al. In vitro cartilage construct generation from silk fibroin-chitosan porous scaffold and umbilical cord blood derived human mesenchymal stem cells in dynamic culture condition. *J Biomed Mater Res A* 2018; 106: 397–407.
25. Röder A, García-Gareta E, Theodoropoulos C, et al. An assessment of cell culture plate surface chemistry for in vitro studies of tissue engineering scaffolds. *J Func Biomater* 2015; 6: 1054–1063.
26. Jones G and Cartmell SH. Optimisation of cell seeding efficiencies on a three-dimensional gelatin scaffold for bone tissue engineering. *J Appl Biomater Biomech* 2006; 4(3): 172–180.
27. García-Gareta E, Hua J, Rayan F, et al. Stem cell engineered bone with calcium-phosphate coated porous titanium scaffold or silicon hydroxyapatite granules for revision total joint arthroplasty. *J Mater Sci Mater Med* 2014; 25(6): 1553–1562.
28. Hori A, Agata H, Takaoka M, et al. Effect of cell seeding conditions on the efficiency of in vivo bone formation. *Int J Oral Maxillofac Implants* 2016; 31(1): 232–239.
29. Boyle DM, Buckley JJ, Johnson GV, et al. Use of the design-of-experiments approach for the development of a refolding technology for progenipoietin-1, a recombinant human cytokine fusion protein from Escherichia coli inclusion bodies. *Biotechnol Appl Biochem* 2009; 54: 85–92.
30. Singh B, Kumar R and Ahuja N. Optimizing drug delivery systems using systematic 'design of experiments'. Part I: fundamental aspects. *Crit Rev Ther Drug Carrier Syst* 2005; 22: 27–105.
31. Thomas RJ, Hourd PC and Williams DJ. Application of process quality engineering techniques to improve the understanding of the in vitro processing of stem cells for therapeutic use. *J Biotechnol* 2008; 136(3–4): 148–155.
32. Kiilll CP, Barud HD, Santagneli SH, et al. Synthesis and factorial design applied to a novel chitosan/sodium polyphosphate nanoparticles via ionotropic gelation as an RGD delivery system. *Carbohydr Polym* 2017; 157: 1695–1702.
33. Jakobsen RB, Ostrup E, Zhang X, et al. Analysis of the effects of five factors relevant to in vitro chondrogenesis of human mesenchymal stem cells using factorial design and high throughput mRNA-profiling. *PLoS ONE* 2014; 9(5): e96615.
34. Ruiter FAA, Alexander C, Rose FRAJ, et al. A design of experiments approach to identify the influencing parameters that determine poly-D,L-lactic acid (PDLLA) electrospun scaffold morphologies. *Biomed Mater* 2017; 12: 055009.
35. Nolte SV, Xu W, Rennekampff HO, et al. Diversity of fibroblasts – a review on implications for skin tissue engineering. *Cells Tissues Organs* 2008; 187(3): 165–176.
36. O'Brien J, Wilson I, Orton T, et al. Investigation of the Alamar blue (resazurin) fluorescent dye for the assessment of mammalian cell cytotoxicity. *Eur J Biochem* 2000; 267(17): 5421–5426.
37. Choi SW, Zhang Y and Xia Y. Three-dimensional scaffolds for tissue engineering: the importance of uniformity in pore size and structure. *Langmuir* 2010; 26(24): 19001–19006.
38. Jafari M, Paknejad Z, Rad MR, et al. Polymeric scaffolds in tissue engineering: a literature review. *J Biomed Mater Res B Appl Biomater* 2017; 105(2): 431–459.
39. Singh D, Singh D, Zo S, et al. Nano-biomimetics for nano/micro tissue regeneration. *J Biomed Nanotechnol* 2014; 10(10): 3141–3161.
40. Christensen BB, Foldager CB, Hansen OM, et al. A novel nano-structured porous polycaprolactone scaffold improves hyaline cartilage repair in a rabbit model compared to a collagen type I/III scaffold: in vitro and in vivo studies. *Knee Surg Sports Traumatol Arthrosc* 2012; 20(6): 1192–1204.
41. Wang S, Kowai TJ, Marei MK, et al. Nanoporosity significantly enhances the biological performance of engineered glass tissue scaffolds. *Tissue Eng Part A* 2013; 19(13–14): 1632–1640.
42. Salmasi S, Kalaskar DM, Yoon WW, et al. Role of nanotopography in the development of tissue engineered 3D organs and tissues using mesenchymal stem cells. *World J Stem Cells* 2015; 7(2): 266–280.
43. Augert A and Bernard D. *Immunosenescence and senescence immunosurveillance: one of the possible links explaining the cancer incidence in ageing population*. London: IntechOpen, 2013.
44. Schneider EL and Mitsui Y. The relationship between in vitro cellular ageing and in vivo human age. *Proc Natl Acad Sci USA* 1976; 73(10): 3584–3588.
45. Pereira MS, Zenki K, Cavalheiro MM, et al. Cellular senescence induced by prolonged subculture adversely affects glutamate uptake in C6 lineage. *Neurochem Res* 2014; 39(5): 973–984.
46. Chen Y, Bloemen V, Impens S, et al. Characterization and optimization of cell seeding in scaffolds by factorial design:

quality by design approach for skeletal tissue engineering. *Tissue Eng Part C* 2011; 17(12): 1211–1221.
47. Nasrollahzadeh N, Applegate LA and Pioletti DP. Development of an effective cell seeding technique: simulation, implementation, and analysis of contributing factors. *Tissue Eng Part C Methods* 2017; 23(8): 485–496.
48. Constantini M, Colosi C, Mozetic P, et al. Correlation between porous texture and cell seeding efficiency of gas foaming and microfluidic foaming scaffolds. *Mater Sci Eng C Mater Biol Appl* 2016; 62: 668–677.
49. Sobral JM, Caridade SG, Sousa RA, et al. Three-dimensional plotted scaffolds with controlled pore size gradients: effect of scaffold geometry on mechanical performance and cell seeding efficiency. *Acta Biomater* 2011; 7(3): 1009–1018.
50. Seebach C, Schultheiss J, Wilhelm K, et al. Comparison of six bone-graft substitutes regarding to cell seeding efficiency, metabolism and growth behaviour of human mesenchymal stem cells (MSC) in vitro. *Injury* 2010; 41(7): 731–738.
51. Marín AC, Brunelli M and Lacroix D. Flow perfusion rate modulates cell deposition onto scaffold substrate during cell seeding. *Biomech Model Mechanobiol* 2018; 17: 675–687.
52. Marín AC, Grossi T, Bianchi E, et al. μ-Particle tracking velocimetry and computational fluid dynamics study of cell seeding within a 3D porous scaffold. *J Mech Behav Biomed Mater* 2017; 75: 463–469.